CARBON 88 (2015) 215–224

Available at www.sciencedirect.com

ScienceDirect

journal homepage: www.elsevier.com/locate/carbon

Quantitative determination of the spatial orientation of graphene by polarized Raman spectroscopy

Zheling Li [a], Robert J. Young [a,*], Ian A. Kinloch [a], Neil R. Wilson [b], Alexander J. Marsden [b], Arun Prakash Aranga Raju [a]

[a] School of Materials, University of Manchester, Oxford Road, Manchester M13 9PL, UK
[b] Department of Physics, University of Warwick, Coventry CV47AL, UK

ARTICLE INFO

Article history:
Received 29 October 2014
Accepted 26 February 2015
Available online 5 March 2015

ABSTRACT

Polarized Raman spectroscopy has been employed to characterize transverse sections of graphene monolayers upon both a copper substrate and a polyester film. Well-defined Raman spectra can be obtained from the one atom thick transverse sections of graphene because of the strong resonance Raman scattering. The intensity of Raman 2D band (I_{2D}) is independent of the axis of laser polarization when the laser beam is perpendicular to the surface of the graphene monolayer but I_{2D} is found to vary as approximately the 4th power of the cosine of the angle between the axis of laser polarization and the plane of graphene when the direction of laser propagation is parallel to the graphene sheet. It is demonstrated that a generalized spherical expanded harmonics orientation distribution function (ODF) can be used to quantify the spatial orientation of the graphene. The roughness of the graphene, evaluated using atomic force microscopy, shows a good correlation with the ODF determined using polarized Raman spectroscopy, showing how the Raman technique may be employed to quantify the spatial orientation of graphene. It is also demonstrated how the technique can be used to quantify the orientation of graphene in high-ordered pyrolytic graphite and graphene paper.

1. Introduction

The spatial orientation of graphene is of great importance because of its two-dimensional geometry and properties such as high strength [1] and high carrier mobility [2]. Such properties can be affected by the spatial orientation of the graphene itself and also an uneven topography, such as wrinkles, is known to affect the properties of graphene dramatically [3–6].

The technique of Raman spectroscopy has been used extensively to study structural features of graphene such as the stacking order [7,8], the presence of defects [9] and the state of oxidation [10]. It has been demonstrated that the deformation of graphene can be monitored from stress-induced Raman band shifts [11–13] and that this phenomenon can then be used to follow the micromechanics of deformation of graphene in nanocomposites [14–17]. A

* Corresponding author.
E-mail address: robert.young@manchester.ac.uk (R.J. Young).
http://dx.doi.org/10.1016/j.carbon.2015.02.072
0008-6223/

dependence of the intensity of the Raman bands upon the direction of laser polarization has been observed in a variety of studies upon graphene structure [18–21]. In particular, the intensity of the D band follows a $\sim\cos^4$ dependence upon the angle of laser polarization relative to a graphene edge, being a maximum when the direction of polarization is parallel to the flake edge [18]. Such studies, however, have taken place with the laser beam of the Raman spectrometer aligned perpendicular to the surface of graphene, so only the in-plane orientation (crystallographic orientation) is revealed [18–21].

Raman spectra have been obtained from transverse section of multilayer graphene or graphite crystals in order to study the spatial orientation [22–24] and it is found that the intensity of Raman bands also follow an approximate $\sim\cos^4$ dependence upon the angle of laser polarization relative to the graphene edge plane. In reality, however, the intensity does not generally fall to zero even when the laser polarization is at 90° to the graphene plane edge due to misalignment or waviness of the scattering entities. Similar behavior has been observed in carbon nanotubes (CNTs) [25–28]. It was shown by Liu and Kumar [29] that it is possible to quantify the spatial orientation distribution function (ODF) of a distribution of aligned CNTs in a similar way to which the ODF can be used to analyze orientational order in polymers [30]. Although the simple concept of the depolarization ratio [31] gives a straight forward idea on the orientation of graphene [24,32], it fails to represent the general spatial ODF. Furthermore, the previous orientation studies were based on multilayer graphene or graphene nanocomposites [22–24,32], and there has been no systematic study to determine the spatial orientation of monolayer graphene, taking into account its surface roughness.

In this present study, the approach of Liu and Kumar [29] to quantify the orientation of CNTs has been modified for the quantitative analysis of the spatial orientation of graphene monolayers. Two particular types of specimen were investigated. Firstly, a graphene monolayer grown by chemical vapor deposition (CVD) on the surface of copper foil (graphene-Cu) and secondly CVD graphene grown on copper and then transferred onto a polyester film (graphene-PET). It is shown that in both cases relatively strong Raman spectra obtained from transverse one atom thick sections [33] can be used to quantify the spatial orientation of the graphene without any prior knowledge of the ODF. The broad agreement between the ODF obtained and the level of surface roughness revealed by atomic force microscopy (AFM) confirms that this technique may be employed to characterize the spatial orientation of graphene.

2. Experimental

2.1. Specimen preparation

The graphene-Cu was grown via low-pressure chemical vapor deposition on copper foils (99.9999% purity, 0.025 mm thick, Alfa Aesar product number 10950) [34,35], which were cleaned in acetone and isopropanol prior to use [36]. The foils were heated from room temperature to 1000 °C in a tube furnace with a 1 inch quartz worktube under a hydrogen flow of 2 standard cubic centimetres per minute (sccm), with a resultant pressure of 10^{-2} mbar. The hydrogen flow was maintained constant throughout the growth process. After annealing for 20 min at 1000 °C, 35 sccm of methane was introduced for a further 10 min. The methane flow rate was reduced to 5 sccm while the sample was cooled to 600 °C, after which the gas flow was stopped.

The graphene-PET sample was supplied by Bluestone Global Tech, USA. Since it is a commercial material full details of its manufacture are confidential but some information has been kindly supplied by Bluestone. The graphene was grown on copper using a conventional methane feedstock and it was then transferred onto PET film. It is mainly monolayer graphene but typically contains approximately 1% by area of multilayered regions and also around 1% of holes due to the transfer, which vary depending upon the growth conditions and transfer technique.

The highly-ordered pyrolytic graphite (HOPG) (43834, $10 \times 10 \times 1$ mm) was supplied by Alfa Aesar. The graphene paper was prepared by the direct exfoliation of graphite (Grade 2369, Branwell Graphite Ltd., UK) in N-methyl-2-pyrrolidone (NMP) (M79603, Sigma–Aldrich) [37,38] in a low power ultrasonic bath (32 W, Elmasonic P70H) for 24 h. The resulting suspension was centrifuged (Thermo Scientific Sorvall LEGEND XTR) for 20 min at ~4000 g following vacuum filtration of the supernatant on 47 mm anodisc membranes (pore size 0.1 μm) to form graphene paper. It was then dried overnight at 80 °C in a vacuum oven.

For the polarization tests in X-direction (transverse to the graphene planes), all samples were embedded transversely using commercial polyester-based mounting plastic. The graphene-Cu and graphene-PET specimens were prepared by either cutting and polishing or microtome sectioning to expose the graphene edges. The HOPG and graphene paper specimens were cut and polished to again expose the graphene edges.

2.2. Characterization

Polarized Raman spectra were obtained using Renishaw 1000/2000 spectrometers with a HeNe laser (λ = 633 nm) for the graphene-Cu, HOPG and graphene paper and an Argon ion laser (λ = 514 nm) for graphene-PET, both with a laser spot around 1~2 μm in diameter, using the so-called 'VV' polarization configuration, where the polarization of incident and scattered radiation are parallel to each other. For graphene-Cu and graphene-PET, the spectra were obtained from both the transverse sections and the top surface of the graphene. AFM images were obtained from the surfaces of the graphene on both the graphene-Cu and graphene-PET using a Dimension 3100 AFM (Bruker) in the tapping mode in conjunction with a 'TESPA' probe (Bruker). The waviness of the graphene on the substrates was determined in terms of the distributions of slopes determined from the AFM height scans using Gwyddion AFM analysis software (gwyddion.net). Optical images of the transverse sections were obtained using an Olympus BH Microscope. Scanning electron microscope (SEM) images were obtained for the graphene-Cu using a Zeiss SUPRA 55-VP FEGSEM and a Philips XL 30 FEG microscope for the HOPG and graphene paper. Transmission

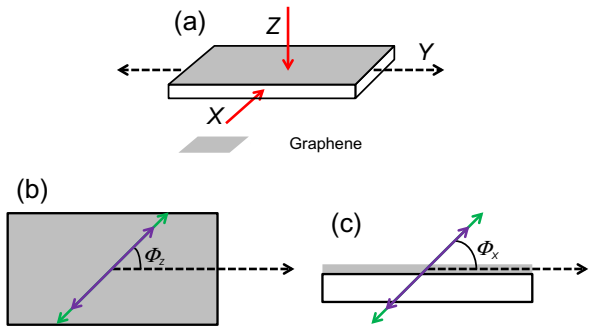

Fig. 1 – Schematic illustration of the relationships between the specimen geometries and polarization arrangements used in the Raman spectroscopic analysis. (a) The specimen in the defined Cartesian coordinate system, and the VV polarization arrangement with the laser beam parallel to the (b) Z or (c) X axis. The red arrow represents the direction of laser propagation and the purple and green arrows represent the directions of polarization of the incident radiation and scattered radiation, respectively (the arrow with the broken line represents the Y direction in all cases). (A color version of this figure can be viewed online.)

electron microscope (TEM) images of the graphene removed from the graphene-Cu were obtained at 200 kV using a JEOL 2000FX with a Gatan Orius camera.

3. Results

3.1. Graphene-Cu

The graphene on the graphene-Cu was shown by a combination of SEM and TEM to consist predominantly of single layer material containing a few wrinkles, with evidence of small amounts of bilayer material (Figs. S1–S3). Polarized Raman spectra were obtained from both transverse section and top surface of the CVD graphene using the 'VV' polarization configuration, with the polarization of incident and scattered radiation both parallel to each other. Fig. 1 defines the Cartesian coordinate system with X, Y and Z axes used to describe the experimental arrangement in which the CVD graphene specimens were examined [39].

The Raman spectra were obtained, first of all, from the graphene with the laser beam parallel to the Z-axis which is perpendicular to the graphene surface. Spectra were then obtained from sections of the specimens with the direction of laser propagation along the X-axis parallel to the plane of the graphene, as shown in Fig. 1. With the polarization configurations fixed, spectra were then obtained with the specimens rotated to different angles, Φ_X and Φ_Z in steps of 10°, for the laser beam parallel to the X and Z directions, respectively.

Fig. 2 shows the results for the polarized Raman analysis of the graphene-Cu. An optical micrograph of a microtome sectioned transverse section of the copper foil is shown in Fig. 2a along with a schematic diagram of the mounted

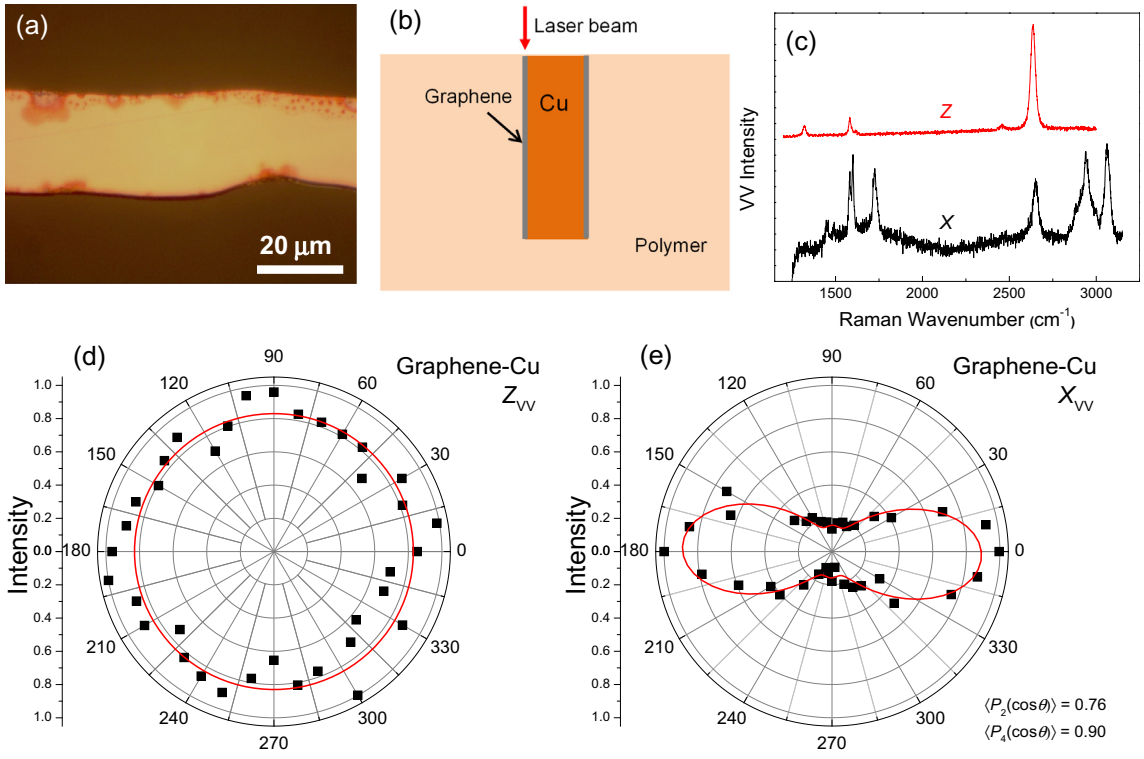

Fig. 2 – (a) Optical micrograph of a microtomed transverse section of the copper foil. (b) Schematic diagram of the transverse section of the copper foil mounted in a polymer resin. (c) Raman spectrum of the graphene-Cu obtained with the laser beam parallel to the Z-axis ($\Phi_Z = 0°$) and the X-axis ($\Phi_X = 0°$) (baseline subtracted), respectively. (d) I_{2D} variation with the laser beam parallel to the Z-axis as a function of the angle Φ_Z. (e) I_{2D} variation with the laser beam parallel to the X-axis as a function of the angle Φ_X. (A color version of this figure can be viewed online.)

specimen in Fig. 2b. The Raman spectrum from the graphene-Cu with the direction of propagation of the laser beam parallel to the Z-axis (perpendicular to the surface of the foil) is shown in Fig. 2c and is a typical spectrum of CVD-grown monolayer graphene [34]. The G band in the spectrum, located at around 1580 cm^{-1}, corresponds to the E_{2g} phonon at the Brillouin zone center (**Γ** point) [2]. The strong 2D band at around 2650 cm^{-1} (also known as the G′ band) results from the two phonons with opposite momentum near the **K** point [7]. The D band centred at around 1300 cm^{-1} and the D′ band at around 1620 cm^{-1}, originate from inter- and intra-valley scattering at the Brillouin zone boundary [40], indicating the presence of defects in the graphene. The high ratio of the intensity of Raman 2D band (I_{2D}) to the intensity of Raman G band (I_G) [41], as well as the sharp 2D band with a full-width at half maximum of less than 35 cm^{-1} are both characteristic of monolayer graphene [42,43].

Fig. 2c also shows the Raman spectrum obtained with the direction of laser propagation parallel to *X* and with $\Phi_X = 0°$. In this case the 2D band is much weaker than with the direction of laser propagation parallel to *Z* but is still observable, similar to the result reported recently from a transverse section of graphene [33]. The G and D bands from the graphene overlap with the Raman bands from the polyester-based mounting polymer. The laser beam is around 2 μm in diameter so most of the light scattered will be from the mounting resin rather than the 0.34 nm thick section of the graphene monolayer, leading to a high fluorescence background. However, the very strong resonant Raman scattering from graphene monolayer enables its Raman spectrum still to be resolved [7].

Finally, the dependence of I_{2D} upon the polarization angle in both axes was determined. The procedure employed to measure the I_{2D} is shown in Fig. S4b. Fig. 2d shows that in the case of the direction of laser propagation parallel to the *Z* axis (i.e. perpendicular to the surface of the graphene) I_{2D} is independent of Φ_Z as expected [18,41]. In contrast in the transverse section, with the direction of laser propagation parallel to the *X* axis, there is strong dependence of I_{2D} upon the angle Φ_X. It is the most intense when $\Phi_X = 0°$ and is a minimum when $\Phi_X = 90°$ and 270° (Fig. 2e). While I_{2D} varies for the graphene-Cu upon rotating in X direction, the intensity of the Raman band from the mounting polymer does not change (Fig. S4a). The same behavior was found when the mounting polymer alone was tested in a similar way (Fig. S4c).

3.2. *Graphene-PET*

A similar analysis was undertaken upon the monolayer graphene-PET as shown in Fig. 3. In this case the graphene 2D band was found to partially overlap with a PET band around 2610 cm^{-1} when excited with the 633 nm laser, so a laser with $\lambda = 514$ nm was used to move the 2D band to a higher wavenumber (Fig. S5b). The Raman scattering from the underlying PET film is strong so that I_{2D} is relatively weak even for the spectrum obtained with the direction of propagation of the laser beam parallel to the *Z* axis (perpendicular to the surface of the film) as shown in Fig. 3c. Nevertheless it can be clearly resolved and is found to be independent of the angle Φ_Z, similar to the behavior of the graphene-Cu shown in Fig. 2d. I_{2D} is relatively weak in the transverse section of the graphene-PET but can still be resolved (Fig. 3d).

A strong angular dependence of I_{2D} upon Φ_X is again obtained for the transverse section (Fig. 3f) although it is difficult to resolve the 2D band from the background scattering

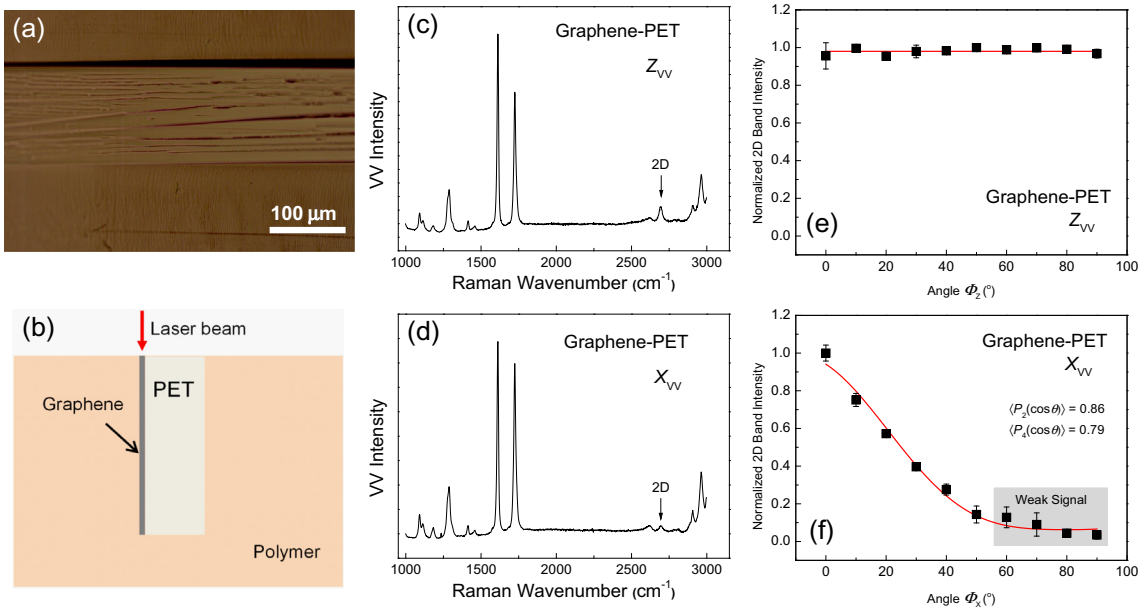

Fig. 3 – (a) Optical micrograph of a microtomed transverse section of the PET film. (b) Schematic diagram of the transverse section of the PET film mounted in a polymer resin. (c) Raman spectrum (baseline subtracted) of the graphene-PET obtained with the laser beam parallel to the Z-axis ($\Phi_Z = 0°$). (d) Raman spectrum (baseline subtracted) of the graphene-PET obtained with the laser beam parallel to the X-axis ($\Phi_X = 0°$). (e) I_{2D} variation with the laser beam parallel to the Z-axis as a function of the angle Φ_Z. (f) I_{2D} variation with the laser beam parallel to the X-axis as a function of the angle Φ_X. (A color version of this figure can be viewed online.)

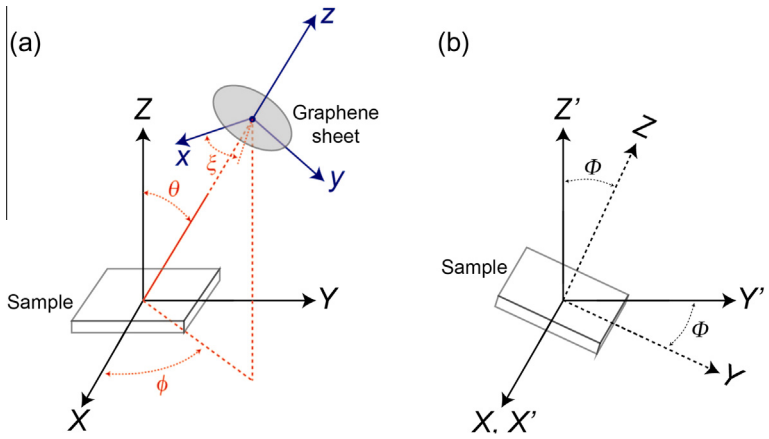

Fig. 4 – Schematic diagrams of the local orientation of graphene within the specimens and of the specimen relative to the experimental polarized Raman spectroscopy measurement parameters. (a) The local coordinate system of the graphene sheet (*x*, *y*, *z*) is related to that of the specimen (*X*, *Y*, *Z*) by the Euler angles (θ, ϕ, ξ). (b) For the polarized Raman spectroscopy measurements described in Fig. 1, the incident and scattered light propagates along the X, X′ axis while the polarization direction of the incident light is in Y′ direction and of the analyzer is in Y′ direction (VV) or Z′ direction (VH). (A color version of this figure can be viewed online.)

above $\Phi_X \sim 60°$ (Fig. S5a). Unlike the graphene-Cu, when the graphene-PET specimen is rotated in X direction, the intensity of the PET Raman band changes as well (Fig. S5a) due to its high degree of molecular orientation [30]. This was also observed when the PET substrate alone was tested in the same way (Fig. S5c).

Previous studies undertaken upon transverse sections of multilayer graphene or graphite crystals [22–24] found that the variation of Raman band intensities with Φ_X for single crystal graphite with a laser beam in the X direction (parallel to the graphene planes) with VV polarization should be of the form:

$$I_{VV}(X) \propto \cos^4 \Phi_X \tag{1}$$

It can be seen from Figs. 2e and 3f that although the data show relationships of this form, the equation is not followed exactly since I_{2D} does not fall to zero at $\Phi_X = 90°$. Eq. (1) can be modified to give a better fit to the experimental data by fitting to an equation of the form

$$I_{VV}(X) \propto C_1 \cos^4 \Phi_X + C_2 \tag{2}$$

where C_1 and C_2 are constants such that $C_1 + C_2 = 1$. A similar relationship was used by Gupta et al. [18] for the intensity variation of the D band with laser polarization angle relative to the edge of a graphene flake to take into account non-uniformity of the edge. Although it is clear that the parameter C_2 will be related to any non-uniform alignment of the graphene, it has no physical significance, meaning that it is impossible to characterize the orientation of the graphene quantitatively using this empirical approach. A more rigorous approach is to quantify the alignment of the graphene in terms of an ODF.

3.3. *Orientation distribution function*

Fig. 4(a) describes the spatial orientation of one graphene flake inside a specimen. The local spatial orientation of a graphene sheet is most conveniently defined by the surface normal vector, shown in Fig. 4(a) as the z-direction with the graphene in the x, y plane. This is related to the coordinate system of the specimen (X, Y, Z) by the Euler angles (θ, ϕ, ξ) as indicated. θ and ϕ are the polar coordinates of z-direction in (X, Y, Z), and ξ is the rotation angle for graphene. Fig. 4(b) is the laboratory coordinates, showing how the specimens were rotated with angle Φ with regard to the laser polarization directions. The incident and scattered light propagate along the X, X′ axis while the polarization direction of the incident light is in Y′ direction and of the analyzer is in Y′ direction (VV) or Z′ direction (VH).

The ODF of the surface normal can be written in general as $f_N(\theta, \phi, \xi)$ such that $f_N(\theta, \phi, \xi)\sin\theta\, d\theta\, d\phi\, d\xi$ is the probability of finding an area element of the graphene with surface normal between (θ, ϕ, ξ) and ($\theta + d\theta$, $\phi + d\phi$, $\xi + d\xi$). Due to the in-plane symmetry of graphene, the rotation angle ξ is not considered. The system is greatly simplified when the ODF shows uniaxial symmetry; i.e. when the orientation of the graphene sheets varies uniformly around a common plane (as is the case for the predominantly flat graphene specimens studied here). In that case the ODF can be written as $f_N(\theta)$. Following Liu and Kumar [29] and van Gurp [44], we can describe any ODF of this kind in terms of Legendre polynomials

$$f_N(\theta) = \sum_{i=0}^{\infty} \frac{2i+1}{2} \langle P_i(\cos\theta)\rangle P_i(\cos\theta) \tag{3}$$

where $P_i(\cos\theta)$ is the Legendre polynomial of the ith degree and $\langle P_i(\cos\theta)\rangle$ is the average value, given by

$$\langle P_i(\cos\theta)\rangle = \frac{\int_{\theta=0}^{\theta=\pi} P_i(\cos\theta) f_N(\theta)\sin\theta d\theta}{\int_{\theta=0}^{\theta=\pi} f_N(\theta)\sin\theta d\theta} \tag{4}$$

The $\langle P_i(\cos\theta)\rangle$ are the order parameters. For most non polar materials the $\langle P_i(\cos\theta)\rangle$ are only non-zero for even *i* and polarized Raman spectroscopy can only be used to determine $\langle P_2(\cos\theta)\rangle$ and $\langle P_4(\cos\theta)\rangle$ [29,45]. The parameter $\langle P_2(\cos\theta)\rangle = (3\langle\cos^2\theta\rangle - 1)/2$ is more commonly known in polymer and composites science as the Herman's orientation factor, S. Generally, the larger the values of $\langle P_2(\cos\theta)\rangle$ and $\langle P_4(\cos\theta)\rangle$,

the better the orientation. $\langle P_2(\cos\theta)\rangle$ is the primary parameter that contains the fundamental information (mean orientation angle) of graphene [45,46]. $\langle P_4(\cos\theta)\rangle$ is less meaningful than $\langle P_2(\cos\theta)\rangle$ with regard to the mean orientation but its value can be used to determine and thus reconstruct the full ODF [46,47]. For example, generally $\langle P_2(\cos\theta)\rangle = (3\langle\cos^2\theta\rangle - 1)/2 = 0$ means the graphene flakes are randomly aligned where $\langle\cos^2\theta\rangle = 1/3$. However, it fails to describe an extreme situation where all the graphene flakes are oriented along the Z axis at an angle θ where $\cos^2\theta = 1/3$ thus $\langle\cos^2\theta\rangle = 1/3$. In this circumstance, the introduction of $\langle P_4(\cos\theta)\rangle$ is of great importance to characterize the orientation fully.

The polarized Raman scattering intensity is given by

$$I \propto \Sigma_i \left| \vec{e}_S \cdot \alpha_i \cdot \vec{e}_I \right|^2 \tag{5}$$

where $\vec{e}_I$ and $\vec{e}_S$ are unit vectors in the direction of the polarization of the incident and scattered light, respectively, and α_i is either the derivative of the polarizability tensor for conventional Raman scattering or the polarizability tensor for resonant Raman scattering [31]. We make the assumption that for 2D band, which is an A_{1g} vibrational mode, α is isotropic within the plane of the graphene and 0 out of the plane since the scattering is due to in-plane phonons [48]. Therefore, in the local (x, y, z) coordinate system, α is given by [49]:

$$\alpha = \begin{pmatrix} 1 & 0 & 0 \\ 0 & 1 & 0 \\ 0 & 0 & 0 \end{pmatrix} \tag{6}$$

For the Raman G band, which is an E_{2g} vibrational mode, the polarizability tensor is given according to [41,49]:

$$E_{2g}(1) = \alpha_1 = \begin{pmatrix} 1 & 0 & 0 \\ 0 & -1 & 0 \\ 0 & 0 & 0 \end{pmatrix} \quad \text{and} \quad E_{2g}(2) = \alpha_2 = \begin{pmatrix} 0 & 1 & 0 \\ 1 & 0 & 0 \\ 0 & 0 & 0 \end{pmatrix} \tag{7}$$

Transforming $\vec{e}_I$ (the Y′ direction in Fig. 4) and $\vec{e}_S$ (either the Y′ direction for VV or Z′ for VH) into the (x, y, z) coordinate system we find that the intensity of the Raman scattering from the graphene sheet in VV polarization is

$$I_{gr}^{VV} \propto \left[\cos^2\phi\cos^2\Phi + (\cos\theta\cos\Phi\sin\phi - \sin\theta\sin\Phi)^2\right]^2 \tag{8}$$

To calculate the total Raman scattering intensity of the specimen, the intensity from all orientations of graphene must be added, giving

$$I_{sample}^{VV} \propto \frac{\int_{\xi=0}^{2\pi}\int_{\phi=0}^{2\pi}\int_{\theta=0}^{\pi} I_{gr}^{VV} f_N(\theta)\sin\theta\,d\theta\,d\phi\,d\xi}{\int_{\xi=0}^{2\pi}\int_{\phi=0}^{2\pi}\int_{\theta=0}^{\pi} f_N(\theta)\sin\theta\,d\theta\,d\phi\,d\xi} \tag{9}$$

Substituting the definition of the ODF (Eqs. (3) and (8)) into Eq. (9) gives the following equation for the Raman scattering intensity of the specimen as a function of the polarization angle Φ relative to the specimen:

$$I_{sample}^{VV}(\Phi) = I_o \cdot \left\{\frac{8}{15} + \langle P_2(\cos\theta)\rangle\left(-\frac{16}{21} + \frac{8}{7}\cos^2\Phi\right) + \langle P_4(\cos\theta)\rangle\left(\frac{8}{35} - \frac{8}{7}\cos^2\Phi + \cos^4\Phi\right)\right\} \tag{10}$$

where the constant I_o is the amplitude. By fitting Eq. (10) to the experimental data, the parameters $\langle P_2(\cos\theta)\rangle$ and $\langle P_4(\cos\theta)\rangle$ can be determined for both specimens (Figs. 2e and 3f). Because of the difficulty in determining the exact alignment of graphene in graphene-Cu and graphene-PET specimens, an offset angle Φ_0 was added in the curve fitting and constrained as $-10° < \Phi_0 < 10°$ (angle Φ_0 was not added into Eq. (10) as it was not considered in the curve fitting of HOPG and graphene paper described later as their alignments can be determined).

As explained by van Gurp [44], these parameters are constrained as: $-1/2 \leqslant \langle P_2(\cos\theta)\rangle \leqslant 1$, $-3/7 \leqslant \langle P_4(\cos\theta)\rangle \leqslant 1$, $\langle P_4(\cos\theta)\rangle \geqslant \frac{1}{18}(35\langle P_2(\cos\theta)\rangle^2 - 10\langle P_2(\cos\theta)\rangle - 7)$ and $\langle P_4(\cos\theta)\rangle \leqslant \frac{1}{12}(5\langle P_2(\cos\theta)\rangle + 7)$. It is noteworthy that Eq. (10) is applicable to both the E_{2g} mode G band and A_{1g} mode 2D band as identical results are generated regardless the polarizability tensors used in the calculation, so the values of $\langle P_2(\cos\theta)\rangle$ and $\langle P_4(\cos\theta)\rangle$ can be determined using either of the two bands. The E_{2g} mode G band is doubly degenerate, and the $E_{2g}(1)$ and $E_{2g}(2)$ tensors correspond to two different in-plane vibrations with perpendicular directions [11]. In terms of the orientational study of graphene in this work, the G band intensity results from both of the in-plane polarizability tensors, with equivalent importance. Therefore both tensors were used in the calculation and the individual G band intensities were summed after calculation from their tensors using Eq. (5). The deduction for the VH polarization configuration is also shown in Supplementary data, but is different from that for the VV polarization. Hence the equation for the E_{2g} mode G band in the VH polarization differs from that of the A_{1g} mode 2D band.

It should be noted that when the graphene is perfectly aligned in the specimen, here equivalent to being perfectly flat, $\langle P_2(\cos\theta)\rangle = \langle P_4(\cos\theta)\rangle = 1$, then Eq. (10) reduces to $I_{sample}^{VV}(\Phi) \propto \cos^4\Phi$. Eqs. (S1) and (S2) similarly reduce to $I_{sample}^{VH}(\Phi) \propto \cos^2\Phi - \cos^4\Phi\ (= \sin^2\Phi\cos^2\Phi)$. Previous orientational studies of graphene and related materials show angular dependencies of these general forms, when the laser beam is either perpendicular ($\theta = \pi/2$ and $\phi = 0$) [18–21] or parallel ($\theta = 0$) to the graphene flakes [22–24].

3.4. HOPG and graphene paper

The analysis was extended to HOPG, which is known to have a crystalline graphite structure [50], and also to graphene paper made by solvent exfoliation and vacuum filtration.

The Raman spectra of HOPG obtained for the laser beam in the Z and X directions with Φ_Z and $\Phi_X = 0°$ are shown in Fig. 5a. The presence of the D and D′ bands for the laser beam in the X direction is due to the discontinuities at the edges of the graphene flake that can be regarded as defects [51]. The D and D′ bands are absent with the beam in the Z direction because the HOPG basal planes are relatively defect-free. The 2D band of HOPG can be fitted with two components, the 2D1 and 2D2 bands.

The intensity variation of the G, 2D1 and 2D2 bands of HOPG with respect to the direction of laser polarization in both X and Z directions are shown in Fig. 5b. This is very similar to the behavior of the I_{2D} of graphene-Cu and graphene-PET. The consistency between the intensity variation of G,

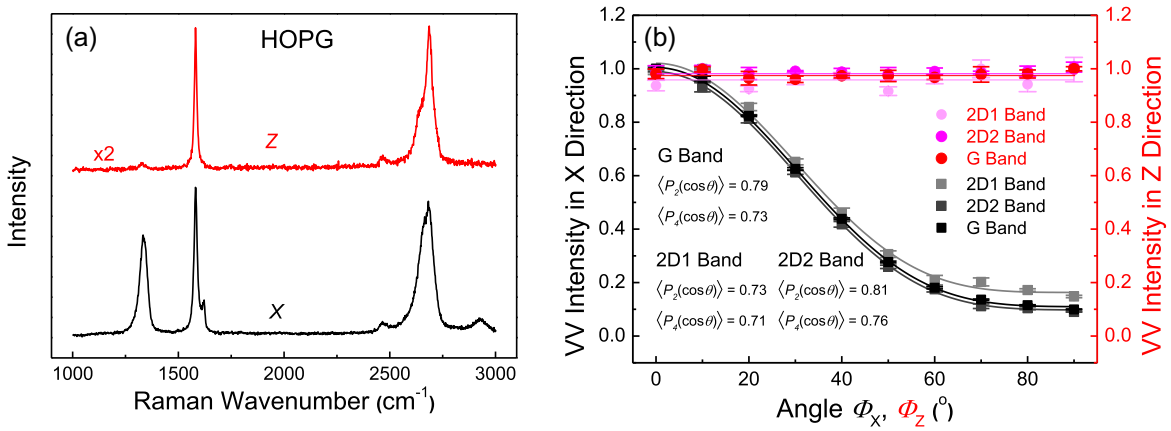

Fig. 5 – (a) Raman spectra and (b) the intensity variation of the G, 2D1 and 2D2 band of HOPG with the angle $\Phi_X(\Phi_Z)$ with the laser beam in both Z and X directions. (A color version of this figure can be viewed online.)

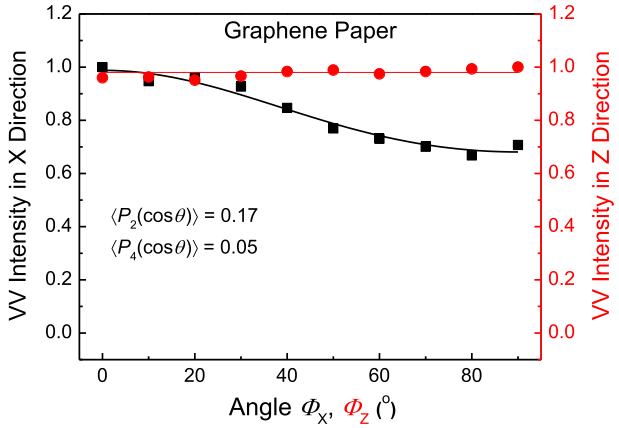

Fig. 6 – I_G variation for laser beam propagation in X and Z directions of graphene paper. (A color version of this figure can be viewed online.)

2D1 and 2D2 band further confirms that Eq. (10) is identical for both the E_{2g} mode G band and the A_{1g} mode 2D band. The small deviation found between the G band and 2D1 band may be due to the 2D1 band being partially from randomly-aligned graphene layers while well-aligned graphene layers contribute to the higher wavenumber 2D2 band [52,53].

The structure of graphene paper was also examined using polarized Raman spectroscopy, and the G band was used here because its 2D band is asymmetric. The variation of I_G with the polarization orientation angle $\Phi_X(\Phi_Z)$ is presented in Fig. 6. The significantly lower values of $\langle P_2(\cos\theta)\rangle$ and $\langle P_4(\cos\theta)\rangle$ in X direction imply a lower level of alignment of the graphene flakes in the paper than for the other materials.

Table 1 – Values of the orientation order parameters determined for the four specimens.

Material	$\langle P_2(\cos\theta)\rangle$	$\langle P_4(\cos\theta)\rangle$
Graphene-Cu	0.85 ± 0.12	0.94 ± 0.05
Graphene-PET	0.76 ± 0.14	0.83 ± 0.05
HOPG	0.79 ± 0.01	0.73 ± 0.02
Graphene paper	0.17 ± 0.01	0.05 ± 0.05

4. Discussion

The average values of $\langle P_2(\cos\theta)\rangle$ and $\langle P_4(\cos\theta)\rangle$ of the materials studied are summarized in Table 1. Based on this, a best guess of the actual ODF can be calculated following the maximum entropy approach as: [29,44]

$$f_N(\theta) = A\exp\left[-(\lambda_2 P_2(\cos\theta) + \lambda_4 P_4(\cos\theta))\right] \quad (11)$$

where the coefficients A, λ_2 and λ_4 are found by numerically solving for them in three simultaneous equations (Eqs. S(4)–S(6)). Fig. 7 shows the calculated ODFs for the four specimens normalized to their corresponding 0° values.

The good alignment of the graphene flakes in HOPG is further confirmed by the SEM image (Fig. S8a), which leads to the ODF of the HOPG being almost same that of the monolayer graphene (Fig. 7). In contrast, the alignment of graphene flakes in the graphene paper is significantly lower (Fig. S8b), which is also reflected by the lower values of $\langle P_2(\cos\theta)\rangle$ and

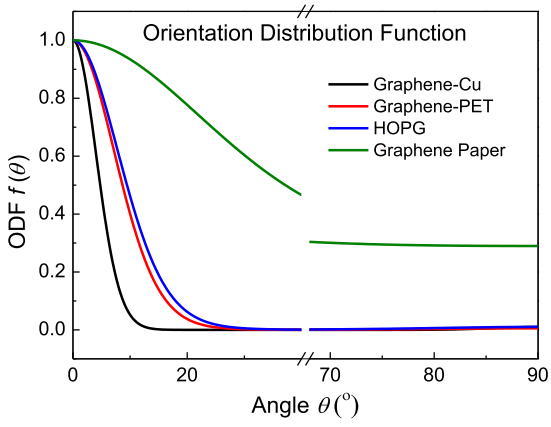

Fig. 7 – ODFs of the four specimens constructed with the measured orientation parameters $\langle P_2(\cos\theta)\rangle$ and $\langle P_4(\cos\theta)\rangle$. (A color version of this figure can be viewed online.)

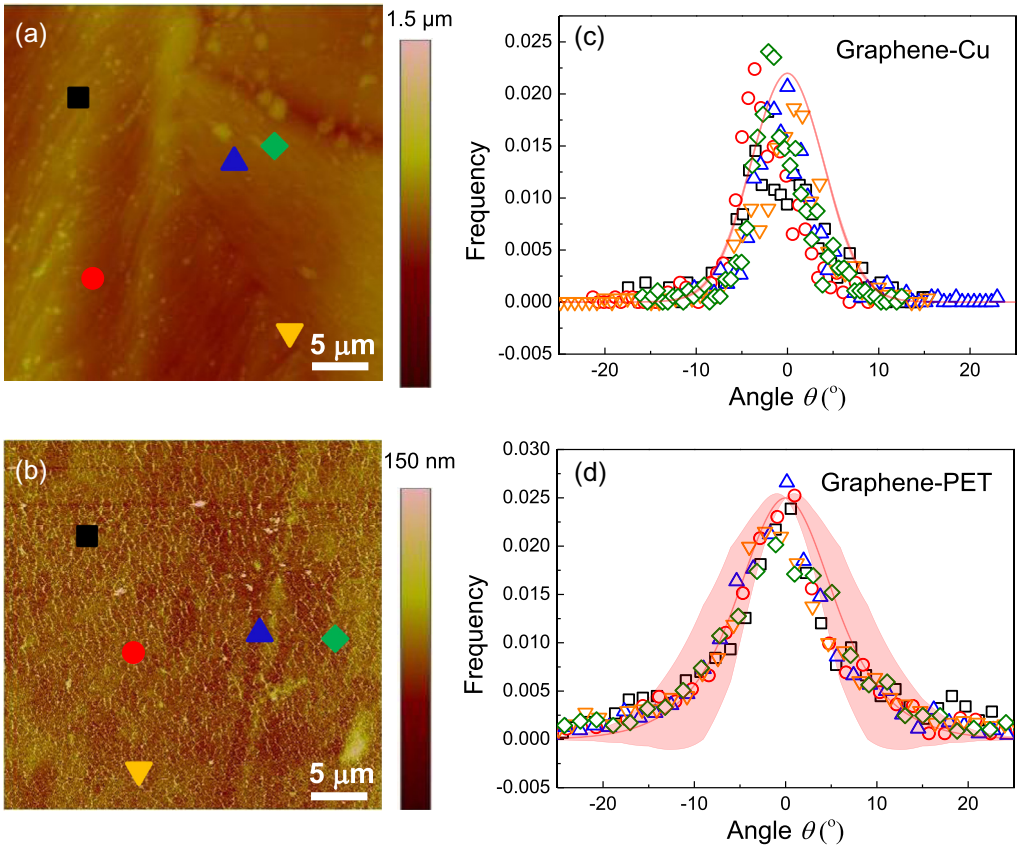

Fig. 8 – AFM analysis of the monolayer graphene on the substrates. Height scans of (a) graphene-Cu and (b) graphene-PET. (c) and (d) Frequency distributions of the angle θ of the local slopes of the graphene on the substrates determined from the AFM height scans. The colored symbols correspond to the data obtained from the five ~2 μm square regions, the positions of which are indicated in Fig. 8a and b. The red lines in the shaded regions in Fig. 8c and d are the average ODFs calculated from the polarized Raman measurements in Figs. 2e and S10a for graphene-Cu, and in Figs. 3f and S10b for graphene-PET. The red shaded regions correspond to the standard deviations. (A color version of this figure can be viewed online.)

$\langle P_4(\cos\theta)\rangle$, possibly due to the small lateral dimension of the graphene [54].

It is interesting to observe that for both monolayer graphene specimens (graphene-Cu and graphene-PET) $\langle P_2(\cos\theta)\rangle$ and $\langle P_4(\cos\theta)\rangle < 1$ which means that in both cases the graphene is not exactly flat. In order to investigate this phenomenon, the topography of the graphene surfaces was studied using AFM by taking height scans in different directions (Figs. 8 and S9). In Fig. 8a, it can be seen that the graphene monolayer follows the topography of the copper surface and so local Cu terraces or Cu grain boundaries will affect the flatness of the graphene [36]. In the case of the graphene-PET specimen it can be seen from Fig. 8b that the graphene on the PET is wrinkled. This may be due to factors such as differential thermal contraction or the process of transferring the graphene from the original substrate to the PET. Fig. 8c and d show histograms of the local slope across the specimen surfaces determined from the AFM tapping-mode height scans across the graphene-Cu and graphene-PET surfaces, respectively, indicating the irregularity in the topography of the graphene. The local slope of the surface at each measurement point was computed using the Gwyddion software and the distribution of the angle θ corresponding to the tangent of the slope was determined. The open symbols in different colors correspond to the data obtained from the five ~2 μm square regions indicated as solid symbols in Fig. 8a and b. These regions are approximately the same size as the Raman laser spot and the similarity between the AFM distributions and ODFs shows that the local roughness can be probed using Raman spectroscopy.

The ODFs determined using the maximum entropy approach for each of the specimens from the polarized Raman spectroscopic data are also plotted in Fig. 8c and d. The Raman orientation measurements were repeated for both graphene-Cu and graphene-PET (Fig. S10), and both sets of data for each material were used to reconstruct the average ODF as shown as the red shaded regions in Fig. 8c and d. The red shaded region in Fig. 8c is very narrow since the value of $\langle P_4(\cos\theta)\rangle$ is close to 1 for the graphene-Cu. It is broader for the graphene-PET in Fig. 8d since the ODF is more sensitive to variations in $\langle P_4(\cos\theta)\rangle$ when it has a value of around 0.8. It can be seen that there is good correlation between the AFM data and the ODFs determined using polarized Raman spectroscopy. Although the surface of graphene-Cu appears to be rougher than that of graphene-PET, the standing wrinkles affect the orientation of the generally flat surface more

severely, as indicated in the broader distribution curves determined from both Raman and AFM data (Fig. 8c and d). This gives confidence in the use of the polarized Raman technique to quantify the orientation of the graphene. Moreover, it confirms that the use of the Legrendre polynomial expansion provides a general but rigorous approach that does not require prior knowledge of the ODF.

5. Conclusions

It has been demonstrated that well-defined Raman spectra can be obtained from transverse sections of graphene monolayers, only one atom thick, as a result of its strong resonance Raman scattering. It has also been shown that polarized Raman spectroscopy can be used to quantify the spatial orientation of graphene. The analysis has been found to be applicable not only to graphene with a high orientation degree such as on copper foil or polyester film, but also to bulk material such as HOPG and specimens with a lower orientation degree such as graphene paper. In particular, it has been shown that it is possible to characterize the topography of buried graphene monolayers which would otherwise be difficult to access. Hence this analysis should find wide application as a characterization technique of graphene in a variety of different applications ranging from electronic devices to nanocomposites. In particular, it could enable the spatial orientation of graphene platelets in nanocomposites to be quantified and related to the mechanical properties of the materials.

Acknowledgments

The authors are grateful for support from the CSC China Scholarship Scheme (Z. L.), the EPSRC (award no. EP/I023879/1), AFOSR/EOARD (award no. FA8655-12-1-2058) and the European Union Seventh Framework Programme under grant agreement n°604391 Graphene Flagship. They would also like to thank Bluestone Global Tech for supplying the polyester film coated with monolayer graphene.

Appendix A. Supplementary data

Supplementary data associated with this article can be found, in the online version, at http://dx.doi.org/10.1016/j.carbon.2015.02.072.

REFERENCES

[1] Lee C, Wei X, Kysar JW, Hone J. Measurement of the elastic properties and intrinsic strength of monolayer graphene. Science 2008;321(5887):385–8.
[2] Malard LM, Pimenta MA, Dresselhaus G, Dresselhaus MS. Raman spectroscopy in graphene. Phys Rep 2009;473(5–6):51–87.
[3] Zhang Y, Gao T, Gao Y, Xie S, Ji Q, Yan K, et al. Defect-like structures of graphene on copper foils for strain relief investigated by high-resolution scanning tunneling microscopy. ACS Nano 2011;5(5):4014–22.
[4] Yu Q, Jauregui LA, Wu W, Colby R, Tian J, Su Z, et al. Control and characterization of individual grains and grain boundaries in graphene grown by chemical vapour deposition. Nat Mater 2011;10(6):443–9.
[5] Bao W, Miao F, Chen Z, Zhang H, Jang W, Dames C, et al. Controlled ripple texturing of suspended graphene and ultrathin graphite membranes. Nat Nano 2009;4(9):562–6.
[6] Zhu W, Low T, Perebeinos V, Bol AA, Zhu Y, Yan H, et al. Structure and electronic transport in graphene wrinkles. Nano Lett 2012;12(7):3431–6.
[7] Ferrari AC, Meyer JC, Scardaci V, Casiraghi C, Lazzeri M, Mauri F, et al. Raman spectrum of graphene and graphene layers. Phys Rev Lett 2006;97(18):187401.
[8] Gong L, Young RJ, Kinloch IA, Haigh SJ, Warner JH, Hinks JA, et al. Reversible loss of bernal stacking during the deformation of few-layer graphene in nanocomposites. ACS Nano 2013;7(8):7287–94.
[9] Eckmann A, Felten A, Mishchenko A, Britnell L, Krupke R, Novoselov KS, et al. Probing the nature of defects in graphene by Raman spectroscopy. Nano Lett 2012;12(8):3925–30.
[10] Stankovich S, Dikin DA, Piner RD, Kohlhaas KA, Kleinhammes A, Jia Y, et al. Synthesis of graphene-based nanosheets via chemical reduction of exfoliated graphite oxide. Carbon 2007;45(7):1558–65.
[11] Huang M, Yan H, Chen C, Song D, Heinz TF, Hone J. Phonon softening and crystallographic orientation of strained graphene studied by Raman spectroscopy. Proc Natl Acad Sci USA 2009;106(18):7304–8.
[12] Mohiuddin TMG, Lombardo A, Nair RR, Bonetti A, Savini G, Jalil R, et al. Uniaxial strain in graphene by Raman spectroscopy: G peak splitting, Grüneisen parameters, and sample orientation. Phys Rev B 2009;79(20):205433.
[13] Zabel J, Nair RR, Ott A, Georgiou T, Geim AK, Novoselov KS, et al. Raman spectroscopy of graphene and bilayer under biaxial strain: bubbles and balloons. Nano Lett 2011;12(2):617–21.
[14] Gong L, Kinloch IA, Young RJ, Riaz I, Jalil R, Novoselov KS. Interfacial stress transfer in a graphene monolayer nanocomposite. Adv Mater 2010;22(24):2694–7.
[15] Young RJ, Gong L, Kinloch IA, Riaz I, Jalil R, Novoselov KS. Strain mapping in a graphene monolayer nanocomposite. ACS Nano 2011;5(4):3079–84.
[16] Gong L, Young RJ, Kinloch IA, Riaz I, Jalil R, Novoselov KS. Optimizing the reinforcement of polymer-based nanocomposites by graphene. ACS Nano 2012;6(3):2086–95.
[17] Raju APA, Lewis A, Derby B, Young RJ, Kinloch IA, Zan R, et al. Wide-area strain sensors based upon graphene-polymer composite coatings probed by Raman spectroscopy. Adv Funct Mater 2014;24(19):2865–74.
[18] Gupta AK, Russin TJ, Gutiérrez HR, Eklund PC. Probing graphene edges via Raman scattering. ACS Nano 2008;3(1):45–52.
[19] Casiraghi C, Hartschuh A, Qian H, Piscanec S, Georgi C, Fasoli A, et al. Raman spectroscopy of graphene edges. Nano Lett 2009;9(4):1433–41.
[20] Cong C, Yu T, Wang H. Raman study on the G mode of graphene for determination of edge orientation. ACS Nano 2010;4(6):3175–80.
[21] Lee J-U, Seck NM, Yoon D, Choi S-M, Son Y-W, Cheong H. Polarization dependence of double resonant Raman scattering band in bilayer graphene. Carbon 2014;72:257–63.
[22] Liang Q, Yao X, Wang W, Liu Y, Wong CP. A three-dimensional vertically aligned functionalized multilayer graphene architecture: an approach for graphene-based thermal interfacial materials. ACS Nano 2011;5(3):2392–401.
[23] Tan P, Hu C, Dong J, Shen W, Zhang B. Polarization properties, high-order Raman spectra, and frequency asymmetry between stokes and anti-stokes scattering of Raman modes in a graphite whisker. Phys Rev B 2001;64(21):214301.

[24] López-Honorato E, Meadows PJ, Shatwell RA, Xiao P. Characterization of the anisotropy of pyrolytic carbon by Raman spectroscopy. Carbon 2010;48(3):881–90.
[25] Duesberg GS, Loa I, Burghard M, Syassen K, Roth S. Polarized Raman spectroscopy on isolated single-wall carbon nanotubes. Phys Rev Lett 2000;85(25):5436–9.
[26] Hwang J, Gommans HH, Ugawa A, Tashiro H, Haggenmueller R, Winey KI, et al. Polarized spectroscopy of aligned single-wall carbon nanotubes. Phys Rev B 2000;62(20):R13310–3.
[27] Rao AM, Jorio A, Pimenta MA, Dantas MSS, Saito R, Dresselhaus G, et al. Polarized Raman study of aligned multiwalled carbon nanotubes. Phys Rev Lett 2000;84(8):1820–3.
[28] Kannan P, Eichhorn SJ, Young RJ. Deformation of isolated single-wall carbon nanotubes in electrospun polymer nanofibres. Nanotechnology 2007;18(23):235707.
[29] Liu T, Kumar S. Quantitative characterization of SWNT orientation by polarized Raman spectroscopy. Chem Phys Lett 2003;378(3–4):257–62.
[30] Tanaka M, Young RJ. Review polarised Raman spectroscopy for the study of molecular orientation distributions in polymers. J Mater Sci 2006;41(3):963–91.
[31] Gommans HH, Alldredge JW, Tashiro H, Park J, Magnuson J, Rinzler AG. Fibers of aligned single-walled carbon nanotubes: polarized Raman spectroscopy. J Appl Phys 2000;88(5):2509–14.
[32] Yousefi N, Lin X, Zheng Q, Shen X, Pothnis JR, Jia J, et al. Simultaneous in situ reduction, self-alignment and covalent bonding in graphene oxide/epoxy composites. Carbon 2013;59:406–17.
[33] Zaretski AV, Marin BC, Moetazedi H, Dill TJ, Jibril L, Kong C, et al. Using the thickness of graphene to template lateral subnanometer gaps between gold nanostructures. Nano Lett 2015;15(1):635–40.
[34] Li X, Cai W, An J, Kim S, Nah J, Yang D, et al. Large-area synthesis of high-quality and uniform graphene films on copper foils. Science 2009;324(5932):1312–4.
[35] Kim KS, Zhao Y, Jang H, Lee SY, Kim JM, Kim KS, et al. Large-scale pattern growth of graphene films for stretchable transparent electrodes. Nature 2009;457(7230):706–10.
[36] Wilson N, Marsden A, Saghir M, Bromley C, Schaub R, Costantini G, et al. Weak mismatch epitaxy and structural feedback in graphene growth on copper foil. Nano Research 2013;6(2):99–112.
[37] Hernandez Y, Nicolosi V, Lotya M, Blighe FM, Sun Z, De S, et al. High-yield production of graphene by liquid-phase exfoliation of graphite. Nat Nano 2008;3(9):563–8.
[38] Nicolosi V, Chhowalla M, Kanatzidis MG, Strano MS, Coleman JN. Liquid exfoliation of layered materials. Science 2013;340:6139.
[39] Li Z, Young RJ, Kinloch IA. Interfacial stress transfer in graphene oxide nanocomposites. ACS Appl Mater Interfaces 2013;5(2):456–63.
[40] Begliarbekov M, Sul O, Kalliakos S, Yang E-H, Strauf S. Determination of edge purity in bilayer graphene using μ-Raman spectroscopy. Appl Phys Lett 2010;97(3). 031908-3.
[41] Yoon D, Moon H, Son Y-W, Samsonidze G, Park BH, Kim JB, et al. Strong polarization dependence of double-resonant Raman intensities in graphene. Nano Lett 2008;8(12):4270–4.
[42] Chen S, Cai W, Piner RD, Suk JW, Wu Y, Ren Y, et al. Synthesis and characterization of large-area graphene and graphite films on commercial Cu–Ni alloy foils. Nano Lett 2011;11(9):3519–25.
[43] Hao Y, Wang Y, Wang L, Ni Z, Wang Z, Wang R, et al. Probing layer number and stacking order of few-layer graphene by Raman spectroscopy. Small 2010;6(2):195–200.
[44] van Gurp M. The use of rotation matrices in the mathematical description of molecular orientations in polymers. Colloid Polym Sci 1995;273(7):607–25.
[45] Perez R, Banda S, Ounaies Z. Determination of the orientation distribution function in aligned single wall nanotube polymer nanocomposites by polarized Raman spectroscopy. J Appl Phys 2008;103(7):074302–74309.
[46] Chatterjee T, Mitchell CA, Hadjiev VG, Krishnamoorti R. Oriented single-walled carbon nanotubes–poly(ethylene oxide) nanocomposites. Macromolecules 2012;45(23):9357–63.
[47] Bower DI. Orientation distribution functions for uniaxially oriented polymers. J Polym Sci Polym Phys Ed 1981;19(1):93–107.
[48] Proctor JE, Gregoryanz E, Novoselov KS, Lotya M, Coleman JN, Halsall MP. High-pressure Raman spectroscopy of graphene. Phys Rev B 2009;80(7):073408.
[49] Loudon R. The Raman effect in crystals. Adv Phys 1964;13(52):423–82.
[50] Hiura H, Ebbesen TW, Tanigaki K, Takahashi H. Raman studies of carbon nanotubes. Chem Phys Lett 1993;202(6):509–12.
[51] Katagiri G, Ishida H, Ishitani A. Raman spectra of graphite edge planes. Carbon 1988;26(4):565–71.
[52] Cançado LG, Takai K, Enoki T, Endo M, Kim YA, Mizusaki H, et al. Measuring the degree of stacking order in graphite by Raman spectroscopy. Carbon 2008;46(2):272–5.
[53] Barros EB, Demir NS, Souza Filho AG, Mendes Filho J, Jorio A, Dresselhaus G, et al. Raman spectroscopy of graphitic foams. Phys Rev B 2005;71(16):165422.
[54] Lin X, Shen X, Zheng Q, Yousefi N, Ye L, Mai Y-W, et al. Fabrication of highly-aligned, conductive, and strong graphene papers using ultralarge graphene oxide sheets. ACS Nano 2012;6(12):10708–19.